

## ESR experiments on the Kondo insulator CeNiSn

S. Mair, Hans-Albrecht Krug von Nidda, Meike Lohmann, Alois Loidl

### Angaben zur Veröffentlichung / Publication details:

Mair, S., Hans-Albrecht Krug von Nidda, Meike Lohmann, and Alois Loidl. 1999. "ESR experiments on the Kondo insulator CeNiSn." *Physical Review B* 60 (24): 16409–14.  
<https://doi.org/10.1103/PhysRevB.60.16409>.

### Nutzungsbedingungen / Terms of use:

licgercopyright

Dieses Dokument wird unter folgenden Bedingungen zur Verfügung gestellt: / This document is made available under these conditions:

**Deutsches Urheberrecht**

Weitere Informationen finden Sie unter: / For more information see:

<https://www.uni-augsburg.de/de/organisation/bibliothek/publizieren-zitieren-archivieren/publiz/>



## ESR experiments on the Kondo insulator CeNiSn

S. Mair, H.-A. Krug von Nidda, M. Lohmann, and A. Loidl

*Experimentalphysik V, Elektronische Korrelationen und Magnetismus, Institut für Physik, Universität Augsburg,  
D-86135 Augsburg, Germany*

(Received 6 July 1999)

Below a characteristic temperature, due to hybridization effects, Kondo insulators exhibit a gap in the electronic density of states and behave like semiconductors. By using  $\text{Gd}^{3+}$  electron spin resonance, the compound CeNiSn was investigated as a representative of this class. In addition, the metal-to-insulator transition was studied as a function of doping for  $\text{CeNi}_{1-x}\text{Co}_x\text{Sn}$  and  $\text{CeNi}_{1-y}\text{Pt}_y\text{Sn}$ . The linewidth of the Gd resonance yields direct information about the density of states at the Fermi energy. So the size of the gap can clearly be estimated for the pure compound, and the closing of the gap by substitution of Ni by Co or Pt can be followed in detail. These results are compared to measurements of NMR, specific heat, and susceptibility. [S0163-1829(99)02448-0]

### I. INTRODUCTION

In recent years Ce-based intermetallic compounds have been the topic of many studies because of their large variety of ground states, e.g., heavy-fermion behavior, nonfermi liquid behavior near a quantum-critical point, intermediate valency and a metal-to-insulator transition in systems called Kondo insulators. The low-temperature physics of these systems is determined by the hybridization of the localized Ce-4*f* states with the conduction band via exchange interactions (Kondo effect). In heavy-fermion compounds, where the 4*f* ions constitute a sublattice of the crystal, this gives rise to spin fluctuations of the Ce-4*f* moments, which are completely screened below a characteristic temperature  $4\text{ K} \lesssim T^* \lesssim 50\text{ K}$ . Above this temperature these compounds reveal Curie-Weiss behavior, characteristic of local-moment paramagnets. Below  $T^*$  they behave like nonmagnetic metals with strongly enhanced effective electron masses. With increasing hybridization ( $50\text{ K} \lesssim T^* \lesssim 500\text{ K}$ ) not only the spin but also the charge of the Ce ions starts to fluctuate, this effect is known as intermediate valency.

In all these Kondo-lattice compounds, the coherence of the Kondo screening causes a pseudogap within the electronic density of states, which evokes below  $T^*$  near the Fermi energy  $E_F$ .<sup>1</sup> Its width is of the order of  $T^*$ . If this gap develops exactly at  $E_F$  and if the density of states vanishes for zero temperature in the gap, the ground state is insulating. These so called Kondo insulators are still in the focus of recent research activities.

One member of this class is CeNiSn with  $T^* \approx 20\text{ K}$ . With decreasing temperature the electric resistance  $\rho$  shows a drastic increase below 7 K. This can be explained by the opening of an energy gap in the electronic density of states.<sup>2,3</sup> As described in these papers, a serious problem of resistance measurements was the strong dependence of the results on the sample quality, especially on the concentrations of impurities in the required single crystals, and it seemed, that the purest single crystals reveal metallic behavior down to the lowest temperatures. Meanwhile, pure CeNiSn has been established as a semimetal with a small overlap of valence and conduction bands.<sup>4</sup> In this case

the hybridization matrix elements vanish at appropriate places of the Brillouin zone. Therefore the density of states exhibits a very small but finite value in the hybridization gap at the Fermi energy. As bulk materials always strongly depend on stoichiometry, defects, and heterogeneities, an experimental method was required that can measure the gap on a microscopic scale in polycrystalline or powdered samples. Of course we are aware that ground-state properties of many heavy-fermion compounds sensitively depend on stoichiometry and sample-growth conditions. We recall the ground-states of  $\text{CeCu}_2\text{Si}_2$  (Refs. 5–7) and  $\text{UPt}_3$ ,<sup>8–11</sup> which reveal a variety of magnetic and superconducting states in polycrystals and single crystals with marginal differences in the growth conditions. CeNiSn may well be a further candidate of this class. Up to now nuclear magnetic resonance (NMR) and neutron scattering have been used successfully to investigate the gap in CeNiSn.<sup>12–15</sup> Here, we present the electron-spin resonance investigations in this compound. To show that the opening of a gap is an intrinsic property of CeNiSn, we provide experimental evidence that the gap can systematically be suppressed (closed or shifted away from  $E_F$ ) by substituting Co or Pt for Ni.

As the Ce spin relaxes too fast to yield any measurable electron spin resonance (ESR) signal, small amounts of  $\text{Gd}^{3+}$  were doped onto the Ce place as ESR probe. In normal metals the linewidth  $\Delta H$  of the  $\text{Gd}^{3+}$  ESR follows a Korringa relaxation  $\Delta H \propto bT$ , where  $b$  directly measures the electronic density of states at the Fermi energy. It has been shown, that the temperature dependence of the Gd linewidth obeys typical patterns in Ce compounds.<sup>16</sup> In heavy fermions [e.g.,  $\text{CeCu}_2\text{Si}_2$ ,<sup>17</sup>  $\text{CeNi}_2\text{Ge}_2$  (Ref. 18)] the Ce-spin fluctuations yield an additional contribution to the usual Korringa relaxation. In intermediate valent compounds [e.g.,  $\text{CePd}_3$ ,<sup>19</sup>  $\text{CeOs}_2$  (Ref. 20)] the Korringa relaxation is strongly reduced below  $T^*$  because of the reduction of the density of states near  $E_F$ . It is important to note that even a partial reduction of the density of states strongly effects the  $\text{Gd}^{3+}$  relaxation, whereas the electric resistance still exhibits metallic behavior as long as  $N(E_F) \neq 0$ .

In CeNiSn, both spin fluctuations and reduced density of states influence the Gd-ESR. We will see that the

ESR results in pure CeNiSn closely agree with those of NMR experiments, and we present a detailed and systematic investigation of the change of the gap in the electronic density of states when doping Pt or Co on the Ni sites. We find a transition to a purely metallic behavior in Co-doped compounds and to a heavy-fermion behavior for the Pt doped alloys. Hence, in the present paper we could support and extend the results of former investigations on CeNiSn by performing ESR measurements at a wide temperature range from 1.6 to 120 K in high quality polycrystalline samples.

## II. SAMPLE PREPARATION AND EXPERIMENTAL SETUP

Polycrystalline samples of  $\text{Ce}_{0.99}\text{Gd}_{0.01}\text{Ni}_{1-x}\text{Co}_x\text{Sn}$  and  $\text{Ce}_{0.99}\text{Gd}_{0.01}\text{Ni}_{1-y}\text{Pt}_y\text{Sn}$  were melted together stoichiometrically from the elements with a purity better than 99.9% in an argon-arc furnace and annealed for 5 days at 1073 K. X-ray diffraction confirmed the proper  $\text{Co}_2\text{Si}$  structure and did not reveal any parasitic impurity phases. Because of the anisotropy of the paramagnetic susceptibility, which shows a maximum in the crystallographic  $a$  axis, it was possible to orient the samples: The polycrystals were powdered to nearly single crystalline grains by a mortar, embedded in liquefied paraffin, and oriented along the  $a$  axis within a static magnetic field of 17 kOe. The ESR measurements were performed with a Bruker ELEXSYS spectrometer at  $X$ -band frequencies ( $\nu \approx 9$  GHz). For cooling the sample, a continuous-flow helium cryostat (ESR900, Oxford Instruments) was used for temperatures above 4 K and a cold-finger helium-bath cryostat for temperatures below 4 K.

## III. RESULTS

### A. ESR spectra

Electron spin resonance probes the absorbed power  $P_{\text{abs}}$  of a transversal magnetic microwave field with frequency  $\nu$  as a function of the static magnetic field  $H$ . To improve the signal-to-noise ratio, a lock-in technique is used by modulating the static field, which yields the derivative of the resonance signal  $dP_{\text{abs}}/dH$ .

All compounds ( $0 \leq x \leq 0.1$  and  $0 \leq y \leq 0.2$ ) show a single resonance line at about  $g=2$ . A representative result is shown in Fig. 1 as solid line. The spectra were fitted using a Dysonian shape,<sup>21</sup> given by

$$\frac{d}{dH}P_{\text{abs}} \propto \frac{d}{dH} \left[ \frac{\Delta H + \alpha(H - H_{\text{res}})}{(H - H_{\text{res}})^2 + \Delta H^2} + \frac{\Delta H + \alpha(H + H_{\text{res}})}{(H + H_{\text{res}})^2 + \Delta H^2} \right], \quad (1)$$

where  $H_{\text{res}}$  denotes the resonance field and  $\Delta H$  the half linewidth at half of the maximum absorption. In Eq. (1) a Lorentzian line ( $\alpha=0$ ) is modified by the influence of the skin effect, which in metals leads to a mixture of real part (=dispersion  $\chi'_{\text{Gd}}$ ) and imaginary part (=absorption  $\chi''_{\text{Gd}}$ ) of the dynamic susceptibility  $\chi_{\text{Gd}} = \chi'_{\text{Gd}} + i\chi''_{\text{Gd}}$ . The dispersion-to-absorption ratio  $\alpha$  is used as fit parameter  $0 \leq \alpha \leq 1$ . The resonance at  $-H_{\text{res}}$  has to be included, because  $\Delta H$  is in the order of  $H_{\text{res}}$ . The result of a representative fit is shown in Fig. 1 as dashed line.

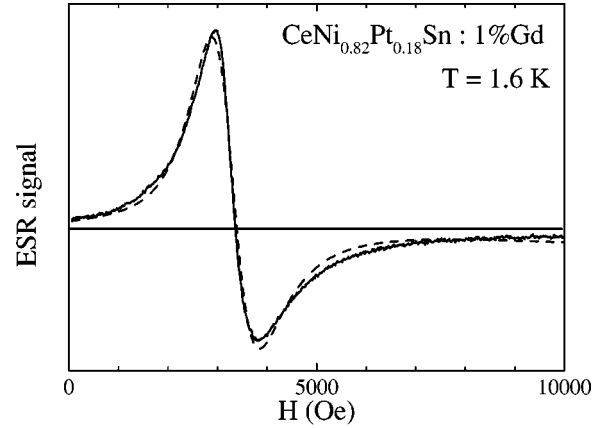


FIG. 1. Typical  $\text{Gd}^{3+}$  ESR spectrum in  $\text{CeNi}_{0.82}\text{Pt}_{0.18}\text{Sn}: 1\% \text{Gd}$  (solid line). The result of a fit, using equation (1) is shown as dashed line.

To understand the origin of the spectra and their dependencies on temperature and orientation, we have to look at the spin Hamiltonian for the  $\text{Gd}^{3+}$  probe in a metallic uniaxial environment, given by<sup>22</sup>

$$\mathcal{H} = \mu_B \mathbf{H} g \mathbf{S} + \frac{1}{3} b_2^0 [3S_z - S(S+1)] + J_{\text{Gd}} \mathbf{S} \cdot \boldsymbol{\sigma}. \quad (2)$$

The first term describes the Zeeman interaction of the Gd spin  $\mathbf{S}$  with the static magnetic field  $\mathbf{H}$  ( $\mu_B$  is the Bohr magneton and  $g$  the gyromagnetic tensor, which is assumed to be isotropic, with  $g \approx 2$ ). The microwave with frequency  $\nu$  induces dipolar transitions between the equidistantly splitted Zeeman levels yielding a single resonance line at  $h\nu = g\mu_B H$ . With respect to the crystal symmetry, the crystal-electric field at the Gd place is assumed to have uniaxial character (parameter  $b_2^0$ ), as described by the second term. This leads to an orientation-dependent splitting of the single spectrum into seven lines due to the Gd spin  $S=7/2$ . The third part of the Hamiltonian is the exchange interaction between the  $\text{Gd}^{3+}$  ion and conduction electrons with spin density  $\boldsymbol{\sigma}$ , where  $J_{\text{Gd}}$  denotes the exchange integral. If the exchange interaction is large compared to the crystal-field splitting, the different dipolar transitions are strongly coupled to each other, and the spectrum is exchange narrowed into a single ESR line with orientation-dependent linewidth and resonance field. For a closer discussion of these effects refer to Ref. 18. The spectra of all samples show only a weak dependence on the orientation. The analysis of the spectra following Ref. 18 results in low values for the uniaxial CEF parameter  $0.3 \text{ GHz} \leq b_2^0 \leq 0.7 \text{ GHz}$ , compared to the microwave frequency  $\nu=9$  GHz. Hence, the influence of the crystal field can be neglected for all further discussion.

### B. Temperature dependence of ESR linewidth

The temperature dependency of the linewidth was measured for samples in the concentration range of interest. Figure 2(a) shows the results for the Pt-doped samples,  $\text{CeNi}_{1-y}\text{Pt}_y\text{Sn}: 1\% \text{Gd}$  for Pt concentrations  $0 \leq y \leq 0.18$ , Fig. 2(b) the Co-doped samples with  $0 \leq x \leq 0.1$ . Looking at the pattern of pure CeNiSn:Gd [Fig. 2(a):  $y=0$ ; Fig. 2(b):

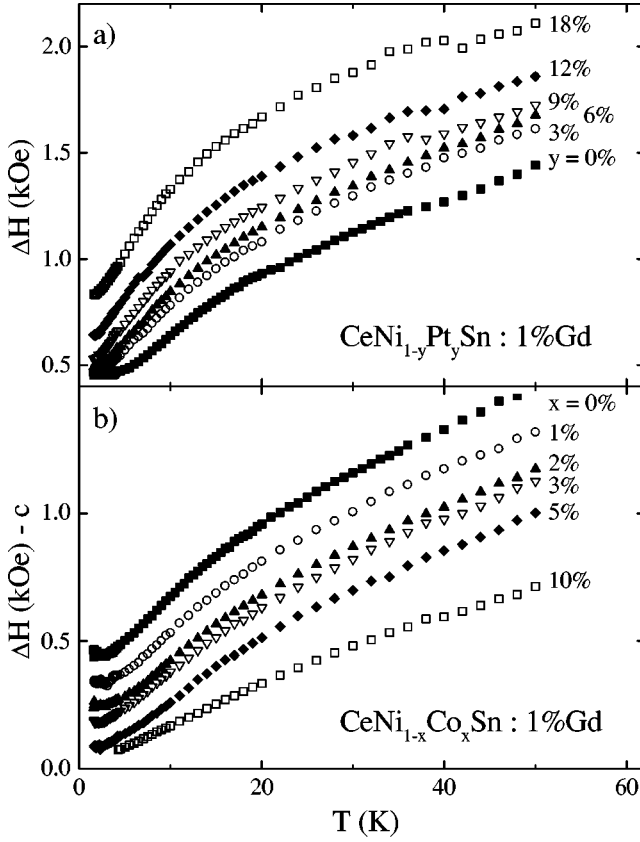


FIG. 2. Linewidth  $\Delta H$  as a function of temperature  $T$  for different concentrations of Pt (top) and Co (bottom). For better clarity the curves in the lower frame are shifted relative to each other by 0.1 ( $x=1\%$ ) to 0.5 ( $x=10\%$ ).

$x=0$ ], we recognize almost a Korringa behavior with a slope  $b$  of about 18 Oe/K for temperatures above 25 K. At lower temperatures the slope increases yielding a gradient  $b \approx 34$  Oe/K for  $5 \text{ K} \leq T \leq 15 \text{ K}$ . At lowest temperatures,  $T < 3 \text{ K}$ , the linewidth becomes almost constant.

Focusing on the  $\text{CeNi}_{1-x}\text{Co}_x\text{Sn}$  compounds [Fig. 2(b)], we recognize, that the high-temperature Korringa slope decreases with increasing Co concentration and also the transition region to an enhanced slope shifts to higher temperatures. The sample with 10% Co shows almost a pure Korringa behavior over the whole temperature range. Substituting Pt for Ni [Fig. 2(a)] enhances the slope between 5 and 15 K and shifts the transition region to lower temperatures. At 18% Pt, the slope of  $\Delta H$  continuously increases towards low temperatures, which is typical for heavy-fermion systems with a rather low characteristic temperature  $T^*$ .<sup>16</sup>

To determine the influence of Gd upon our results, we compared samples with 0.2% and 1% Gd substituted at the Ce places. The temperature dependence of the linewidth for these compounds is shown in Fig. 3 and clearly demonstrates that Gd does not influence the linewidth. So, we can exclude effects like Gd-Gd interaction or bottleneck effects, which are discussed in Ref. 23.

#### IV. DISCUSSION

Generally, the ESR linewidth  $\Delta H$  measures the transversal relaxation rate  $1/T_2$ . Because of very short correlation

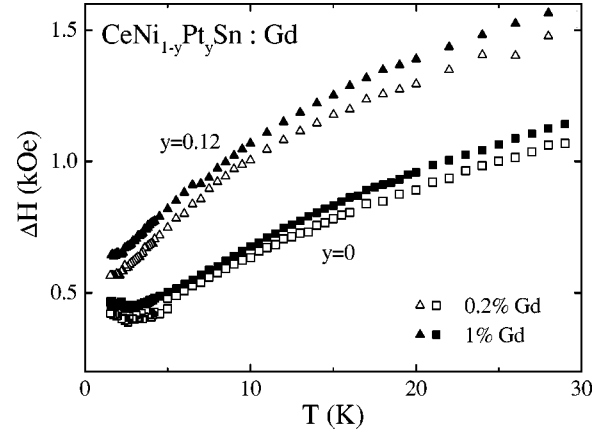


FIG. 3. Linewidth  $\Delta H$  as a function of temperature  $T$  for Gd-concentrations of 1% (solid symbols) and 0.2% (open symbols) for pure  $\text{CeNiSn}:\text{Gd}$  ( $\square$ ) and  $\text{CeNi}_{0.88}\text{Pt}_{0.12}\text{Sn}:\text{Gd}$  ( $\Delta$ ).

times, the longitudinal or spin-lattice relaxation rate  $1/T_1$  equals  $1/T_2$  in metals.<sup>22</sup> In heavy fermions the spin-lattice relaxation of the Gd spins is governed by two mechanism<sup>23,16</sup>

$$\frac{1}{T_1} \propto \Delta H = \Delta H_K + \Delta H_{\text{RKKY}}. \quad (3)$$

The Korringa relaxation  $\Delta H_K$ , which is usually observed in metals, is caused by the third term in Eq. (2). The conduction electrons scatter at the Gd spin and transfer the energy to the lattice. This contribution is proportional to the temperature  $T$  (dash-dotted curve in the upper frame of Fig. 4) and the

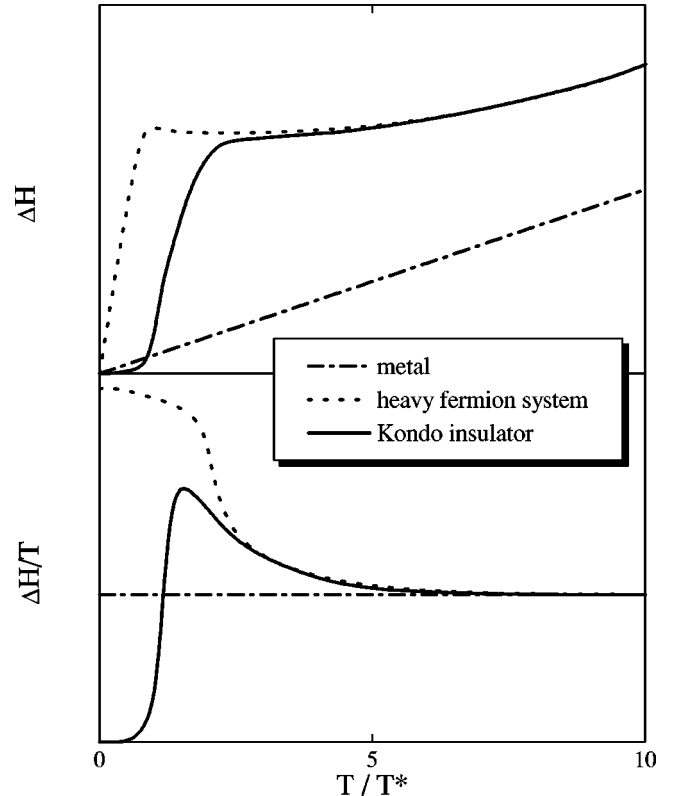


FIG. 4. Simulation of the ESR linewidth of a metal, a heavy-fermion system and a Kondo insulator.

square of the electronic density of states at the Fermi level  $N_{\text{CE}}^2(E_F)$

$$\Delta H_K \propto \langle J_{\text{Gd}}^2(q) \rangle \cdot N_{\text{CE}}^2(E_F) \cdot T := b \cdot T, \quad (4)$$

where  $\langle J_{\text{Gd}}^2(q) \rangle$  is the exchange integral averaged over the momentum transfer  $q$  from the scattering of the conduction electrons at the Gd spin.

The second term  $\Delta H_{\text{RKKY}}$  results from spin fluctuations of the Ce-4*f* moments according to the fluctuation-dissipation theorem. These are transferred to the Gd spin via Rudermann-Kittel-Kasuya-Yosida (RKKY) interactions:

$$\Delta H_{\text{RKKY}} \propto T \chi_{\text{Ce}}^0 \tau \sum_i \lambda_{\text{CeGd}}^2(R_i), \quad (5)$$

where  $\lambda_{\text{CeGd}}$  is the RKKY coupling to the Ce atoms at a distance  $R_i$ .  $\chi_{\text{Ce}}^0$  describes the static Ce susceptibility, which in ideal heavy-fermion systems follows a Curie-Weiss law  $\chi_{\text{Ce}}^0 \propto (T + \Theta)^{-1}$  with  $\Theta = \sqrt{2}T^*$  (Ref. 24) at high temperatures  $T > T^*$  and saturates as a large Pauli-like susceptibility of heavy quasiparticles at  $T \ll T^*$ . For  $T \ll T^*$  the spin-correlation time  $\tau$  of the Ce spins is determined by the characteristic temperature according to  $1/\tau = k_B T^*/\hbar$ . At higher temperatures,  $T > T^*$  it shows a behavior like  $1/\tau \propto \sqrt{T}$ .<sup>25</sup> So, for  $T < T^*$  we expect an additional, strong linear increase of the linewidth  $\Delta H$  with the temperature (dotted curve in the upper frame of Fig. 4).

In contrast to the typical heavy-fermion pattern, for CeNiSn the slope of  $\Delta H(T)$  again decreases at lowest temperatures and approaches zero. A similar behavior was observed in the intermediate valent compounds CePd<sub>3</sub> and CeOs<sub>2</sub>, where the Korringa slope of the Gd linewidth was about 10 times smaller at low temperatures than the Korringa relaxation  $b$  in the respective reference compounds YPd<sub>3</sub> and LaOs<sub>2</sub>.<sup>19,20</sup> This was explained in terms of a reduced density of states of the conduction electrons within a regime  $k_B T^*$  at the Fermi energy. For a quantitative description  $\Delta H_K$  was calculated with an energy-dependent density of states. The contribution  $\Delta H_{\text{RKKY}}$  vanished because of the delocalization of the *f* electrons in intermediate valent systems.

In CeNiSn, however, the contribution of the spin fluctuations cannot be neglected. Therefore, a quantitative description would be much more complicated. Here we confine ourselves to a qualitative argumentation and to comparisons with results of other experimental methods.

The gradual development of a pseudogap in the density of states of both the conduction electrons and the 4*f* electrons below a characteristic temperature is a generic feature, which follows from the coherence of a Kondo lattice.<sup>1</sup> If the pseudogap develops just at the Fermi level, it should reduce the relaxation rate due to  $\Delta H_K$  as well as  $\Delta H_{\text{RKKY}}$ , which both depend on  $N(E_F)$ . Therefore, one expects an *S*-shaped temperature dependence, which is shown as solid curve in the upper frame of Fig. 4. The qualitative agreement of  $\Delta H(T)$  of the measured curve of CeNiSn, shown in Fig. 2, with the model of a Kondo insulator as shown in Fig. 4 is clearly evident.

For further discussion and comparison with NMR, susceptibility and specific-heat experiments, we choose the  $\Delta H/T$  plot, which better pronounces the effect of the

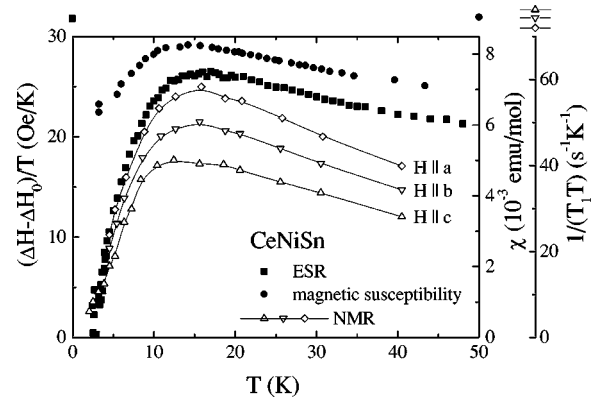


FIG. 5. Comparison of the results of ESR, magnetic susceptibility (Ref. 3), and NMR (Ref. 12).

pseudogap. As can be seen from Eqs. (3)–(5)  $\Delta H/T$  corresponds to the dynamic susceptibility plus a constant effect due to the Korringa slope  $b$ . The theoretical expectations are shown in the lower frame of Fig. 4. Whereas normal metals reveal a constant behavior over the whole temperature range and heavy fermions saturate at a high value at low temperatures, Kondo insulators exhibit a maximum in  $\Delta H/T$  at a temperature  $T_{\text{max}}$ , which is a rough measure for the width of the gap.

Before we apply this plot on our experimental linewidth data, we have to subtract the residual linewidth  $\Delta H_0$ , which is always present in real samples and which is caused by impurities and grating division errors. To obtain  $\Delta H_0$ , one has to extrapolate the linewidth data to zero temperature.

Figure 5 shows  $(\Delta H - \Delta H_0)/T$ , which nicely resembles the expected pattern for a Kondo insulator. The ESR results are compared to  $^{119}\text{Sn}$ -NMR and static susceptibility  $\chi_{\text{Ce}}^0$  results. The  $^{119}\text{Sn}$ -nuclear spin relaxes via Fermi-contact interaction to the conduction electron system. Therefore, an analogous expression to Eq. (3) holds for  $(1/T_1)_{\text{NMR}}$ . The NMR data<sup>3</sup> of  $1/(T_1 \cdot T)$  show a similar behavior as the ESR data. The orientation-dependent measurements are very similar to each other, in particular the position of the maximum, which is a gauge for the gap, does not change with orientation. These data also characterize CeNiSn as a Kondo insulator.

Macroscopic experimental methods like the magnetic susceptibility  $\chi$  prove the microscopic data.<sup>12</sup> The decrease of  $\chi$  for low temperatures can be explained by a reduction of the density of states at the Fermi level. As the correlation time  $\tau$  changes only slightly for  $T < T^* \approx 20$  K,  $(\Delta H - \Delta H_0)/T$  behaves similar to the susceptibility. At low temperatures magnetic impurities may influence the magnetic susceptibility significantly.

To examine the influence of the substitution of Ni by Co or Pt, we use again the  $(\Delta H - \Delta H_0)/T$  plot (Fig. 6). First we see a constant value for the compound with 10% Co, which behaves like a normal metal. The compound with a Pt concentration of 18% shows a constant high value for low temperatures, typical for a heavy-fermion system. All other curves exhibit a behavior like a Kondo insulator with a maximum at temperatures between 5 and 15 K. This maximum shifts to lower temperatures for increasing Pt concentrations, and to higher temperatures for Co doping. As described be-



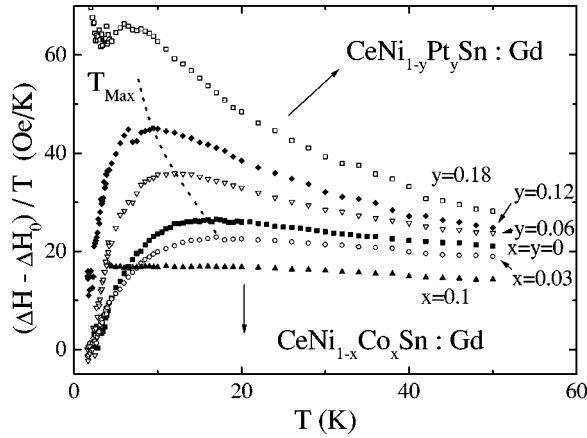


FIG. 6.  $(\Delta H - \Delta H_0)/T$  as a function of temperature for different Co and Pt dopings.

fore, the maximum characterizes the width of the gap in the density of states. However, the right extrapolation to  $\Delta H_0$  is sometimes quite difficult. To avoid a dependence on  $\Delta H_0$ , we therefore introduced a characteristic temperature  $T_c$ , which describes the temperature, at which the bending or second differential on temperature changes from positive to negative sign for increasing temperature. This turning point is characteristic for the size of the gap, too.

To determine the behavior of the gap with an increasing volume of the elementary lattice cell, we substitute Ni by Pt. We clearly see in Fig. 7, that this leads to a decrease of this characteristic temperature from 9 K at pure CeNiSn to 4 K with 9% Pt. Doping small amounts of Co into the samples leads to an increase of the characteristic temperature, indicating an increase of the gap. On the other hand, the behavior of the linewidth gets more linearly. This points to the fact, that the density of states at Fermi level is not zero, but becomes higher and higher for increasing Co concentration. At about 10% Co the gap is completely filled, and the sample behaves like a metal.

Co substitution does not change the size of the elementary cell volume. X-ray measurements revealed, that the lattice parameters remain almost constant for doping up to 10% Co on the Ni sites. The most important effect of the Co seems to be the reduction of the number of electrons. This leads to a destruction of the Abrikosov-Suhl resonance and so of the

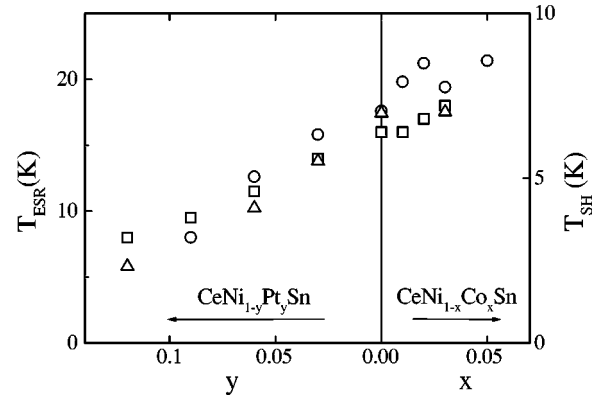


FIG. 7. Characteristic temperature ( $\circ$ , left axis divided by 2) and maximum of  $(\Delta H - \Delta H_0)/T$  ( $\square$ , left axis) of ESR measurements and maximum of  $C_m/T$  ( $\triangle$ , right axis) (Ref. 26) for different concentrations of Co ( $x$ ) and Pt ( $y$ ).

heavy-fermion behavior. Figure 7 also shows data of characteristic temperatures for the gap, got by measurement of specific heat.<sup>26</sup> These data correspond very well to our ESR data.

## V. CONCLUSION

We have shown that Gd-ESR nicely probes the coherence gap in Kondo insulators. The S-shaped temperature dependence of the linewidth in CeNiSn:Gd is comparable to the spin-lattice relaxation rate  $1/T_1$  of  $^{119}\text{Sn}$ -NMR, which both measure the conduction-electron density of states at the Fermi energy. The evolution of the gap by doping Pt or Co onto the Ni site agrees with specific-heat experiments. Pt doping increases the cell volume, hence decreases the hybridization and therefore narrows the gap, whereas Co changes the electron configuration, disturbs the coherence, and the gap is gradually filled and smeared out.

## ACKNOWLEDGMENTS

We are grateful to A. Brand, B. Mayer, S. Saladie, and D. Vieweg for the preparation of the samples and the x-ray measurements. This work was supported by the Bundesministerium für Bildung und Forschung (BMBF) under Contract No. 13N6917/0.

- <sup>1</sup> N. Grewe and F. Steglich, in *Handbook on the Physics and Chemistry of Rare Earths*, edited by K. A. Gschneidner and L. Eyring (Elsevier Science, Amsterdam, 1991), Vol. 14.
- <sup>2</sup> D. T. Adroja, B. D. Rainford, A. J. Neville, and A. G. M. Jansen, *Physica B* **223&224**, 275 (1996).
- <sup>3</sup> T. Takabatake, G. Nakamoto, T. Yoshino, H. Fujii, K. Izawa, S. Nishigori, H. Goshima, T. Suzuki, T. Fujita, K. Maezawa, T. Hiraoka, Y. Okayama, I. Oguro, A. A. Menovsky, K. Neumaier, A. Brückl, and K. Andres, *Physica B* **223&224**, 413 (1996).
- <sup>4</sup> P. S. Riseborough, *Adv. Phys.* (to be published).
- <sup>5</sup> F. Steglich, J. Aarts, C. D. Bredl, W. Lieke, D. Meschede, W. Franz, and H. Schaefer, *Phys. Rev. Lett.* **43**, 1892 (1979).
- <sup>6</sup> C. D. Bredl, H. Spille, U. Rauchschwalbe, W. Lieke, F. Steglich,

- G. Cordier, W. Assmus, M. Herrmann, and J. Aarts, *J. Magn. Mater.* **31-34**, 373 (1983).
- <sup>7</sup> F. Steglich, C. Geibel, R. Modler, M. Lang, P. Hellmann, and P. Gegenwart, *J. Low Temp. Phys.* **99**, 267 (1995).
- <sup>8</sup> G. R. Stewart, Z. Fisk, J. O. Willis, and J. L. Smith, *Phys. Rev. Lett.* **52**, 679 (1984).
- <sup>9</sup> G. Aeppli, E. Bucher, C. Broholm, J. K. Kjems, J. Baumann, and J. Hufnagel, *Phys. Rev. Lett.* **60**, 615 (1988).
- <sup>10</sup> R. Spitzfaden, A. Schuetz, H.-A. Krug von Nidda, B. Elschner, and A. Loidl, *Solid State Commun.* **102**, 445 (1997).
- <sup>11</sup> F. Gandra, M. J. Pontes, S. Schultz, and S. B. Oseroff, *Solid State Commun.* **64**, 859 (1987).
- <sup>12</sup> T. Ohama, H. Yasuoka, and Y. Isikawa, *J. Phys. Soc. Jpn.* **64**, 4566 (1995).

- <sup>13</sup>T. J. Sato, H. Kadowaki, H. Yoshizawa, T. Ekino, T. Takabatake, H. Fujii, L. P. Regnault, and Y. Isikawa, J. Phys.: Condens. Matter **7**, 8009 (1995).
- <sup>14</sup>T. E. Mason, G. Aeppli, A. P. Ramirez, K. N. Clausen, C. Broholm, N. Stücheli, E. Bucher, and T. T. M. Palstra, Phys. Rev. Lett. **69**, 490 (1992).
- <sup>15</sup>A. Schröder, G. Aeppli, T. E. Mason, and E. Bucher, Physica B **234-236**, 861 (1997).
- <sup>16</sup>B. Elschner and A. Loidl, in *Handbook on the Physics and Chemistry of Rare Earths*, edited by K. A. Gschneidner and L. Eyring (Elsevier Science, Amsterdam, 1997), Vol. 24.
- <sup>17</sup>M. Schlott, B. Elschner, H. Herrmann, and W. Assmus, Z. Phys. B: Condens. Matter **72**, 385 (1988).
- <sup>18</sup>H.-A. Krug von Nidda, A. Schütz, M. Heil, B. Elschner, and A. Loidl, Phys. Rev. B **57**, 14 344 (1998).
- <sup>19</sup>H. Schäffer and B. Elschner, Z. Phys. B: Condens. Matter **53**, 109 (1983).
- <sup>20</sup>M. Schlott, H. Schäffer, and B. Elschner, Z. Phys. B: Condens. Matter **63**, 427 (1986).
- <sup>21</sup>F. J. Dyson, Phys. Rev. **98**, 337 (1955).
- <sup>22</sup>S. E. Barnes, Adv. Phys. **30**, 801 (1981).
- <sup>23</sup>M. Coldea, H. Schäffer, V. Weissenberger, and B. Elschner, Z. Phys. B: Condens. Matter **68**, 25 (1987).
- <sup>24</sup>J. Callaway, *Quantum Theory of the Solid State* (Academic Press, New York, 1991), p. 448.
- <sup>25</sup>D. L. Cox, N. E. Bickers, and J. W. Wilkins, J. Appl. Phys. **57**, 3166 (1985).
- <sup>26</sup>S. Nishigori, H. Goshima, T. Suzuki, T. Fujita, G. Nakamoto, H. Tanaka, T. Takabatake, and H. Fujii, J. Phys. Soc. Jpn. **65**, 2618 (1996).